Simulations of the snap-through behavior of a fiber reinforced elastomer structure for the design of a simple clamping mechanism

Marius M. Schasching[1,*]**, Robert Duy**[1]**, Melanie Todt**[1]**,** and **Heinz E. Pettermann**[1]

[1] Institute of Lightweight Design and Structural Biomechanics, TU Wien, Getreidemarkt 9, A-1060 Vienna, Austria

A glass fiber reinforced elastomer (FRE) sheet is used to design a simple clamping mechanism for prospective engineering applications. The mechanism is based on the phenomena of snap-through buckling of a segment of a shallow cylindrical shell. It is simply supported at the straight edges and actuated by edge moments. The main objective of such a mechanism is the resulting clamping force, being related to the response of the material under bending. Bending includes compressive stresses, and since the fibers are embedded in a very soft matrix, it is important to understand their contribution to the compressive stiffness of the FRE sheet. For this purpose, numerical simulations by means of the Finite Element Method are performed and a simulation strategy for predicting the clamping force of the mechanism is presented. The clamping forces predicted for FRE composites with and without the contribution of fibers to the compressive stiffness are compared to that of the pure elastomer. The results illustrate the potential of FRE based structures in mechanism-like applications. If an adequate clamping force is desired, the pure elastomer is not suitable for being used in this kind of clamping mechanism and the fiber reinforcement is necessary. If the fibers contribute to the compressive stiffness, a significantly higher clamping force is predicted. Furthermore, the FRE based structure shows a complex snap-through deformation pattern, which has to be taken into account in the design of the mechanism and which requires non-trivial simulation strategies.

1 Introduction

Soft grippers are becoming more and more interesting in various prospective engineering fields [11]. The actuation of such grippers can be based on various stimuli such as electrical and mechanical. For mechanical actuation, it is often necessary to keep the actuation active to ensure operation as, e.g., for the concept presented in [5]. Therein, the actuation is performed by pneumatically pressurizing silicone chambers. In order to keep the clamping force of the gripper active, the pressure cannot be released. To overcome this issue, mechanical bistability can be exploited instead, where two stable states correspond to either an active or an inactive clamping force. Bistability can be achieved on the basis of snap-through buckling of a shallow cylindrical shell segment, e.g., as shown in [7, 10] with piezoelectric actuation. The snap-through behavior of cylindrical shell segments to occur is strongly influenced by various parameters such as geometrical dimensions, boundary conditions, and material. Small variations of these parameters can significantly change the instability response, and local buckling rather than snap-through can become the prevailing type of instability. Besides, the choice of material is not only critical for the snap-through behavior, but also to meet the requirements of a soft gripper. The material needs to show sufficient flexibility to avoid harming the target object and sufficient stiffness to provide an adequate clamping force. Therefore, a fiber reinforced elastomer (FRE) is intended to be employed, which has recently been developed at Polymer Competence Center Leoben (PCCL), Austria, [1–3]. Since the fibers are embedded in a very soft matrix, it is important to understand their contribution to the response of the material especially under compressive stress states.

In this work, a concept for a simple clamping mechanism based on the snap-through behavior of a shallow cylindrical shell segment is aimed for, using available FRE sheets. For this purpose, numerical simulations by means of the Finite Element Method (FEM) are performed and a simulation strategy for predicting the clamping force of the mechanism is presented. All simulations are performed with ABAQUS 2020/Standard (*Dassault Systèmes Simulia Corp., Providence, RI, USA*).

2 Concept of mechanism

The snap-through instability of a shallow cylindrical shell segment is employed to obtain a mechanism with bistable character. The goal is to enable switching between two stable configurations by applying a certain actuation. Once a stable configuration is reached, the actuation can be released while the structure applies a retaining but reversible force against a rigid body to clamp a target object in between. The material used for the mechanism is a FRE, which is composed of pure silicone as matrix material and glass fibers as reinforcement. The reinforcement is a 2/2 twill weave with fibers uniformly distributed in the 0° and 90° direction. The FRE shows orthotropic hyperelastic material behavior with equal properties in both fiber directions. When dealing with the snap-through behavior of cylindrical composite shells using a transverse point load, it has been shown that the material orthotropy acts as a driver for a more complex stability behavior [8], even though it has already been shown to be quite complex for isotropic materials in [12]. Therefore, a more distributed loading condition is aimed for in the current concept to reduce complexity while being technically feasible.

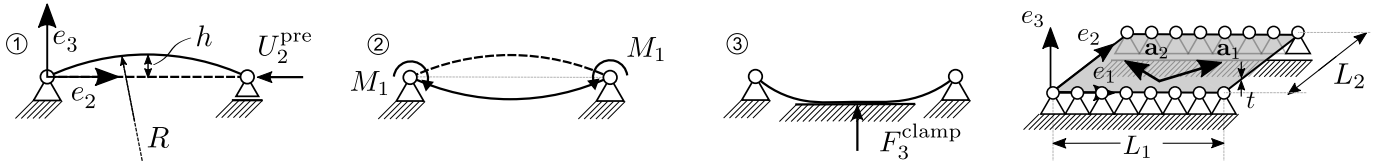* Corresponding author: e-mail marius.schasching@tuwien.ac.at,

Fig. 1: Schematic of the concept of the mechanism in 2D and dimensions of the sheet with fiber orientation vectors $\mathbf{a}_1$ and $\mathbf{a}_2$ in 3D.

L_1 in mm	L_2 in mm	t in mm	n_1 -	n_2 -
50	50	0.5	20	20

Table 1 Geometrical dimensions of the analyzed sheet, cf. Figure 1, where L_1 and L_2 denote the length in 1- and 2-direction, respectively, and t is the thickness of the sheet. The number of finite elements used along 1- and 2-direction is given by n_1 and n_2, respectively.

The concept of the mechanism is schematically depicted in Figure 1. For simple production of the FRE, the curved shell structure shall be obtained from a flat sheet, which can readily be manufactured at PCCL, Austria. First, the curvature is realized by applying an in-plane displacement in 2-direction, U_2^{pre}, at one of the edges of the simply supported sheet, causing it to buckle. The obtained curved shell structure corresponds to the first stable configuration with apex, h, and radius, R. Second, torque loads, M_1, on both edges are applied to let the structure snap-through and to switch to the second stable configuration. Subsequently, the torque loads can be released. Third, the contact with a target object is established, once a second stable configuration is entered. The resulting reaction force between structure and target object is directly related to the resulting clamping force, F_3^{clamp}, of the mechanism.

For the current concept, the clamping force is related to the material response under bending. Bending results in either tensile or compressive stress states on one side of the neutral axis at a time. For compressive stress states, the contribution of the fibers is vague as they are embedded in a soft matrix. Local buckling may occur leading to a more compliant material behavior. This can influence the overall mechanical behavior of the structure and, consequently, affect the clamping force. Hence, studying the contribution of fibers to the structural response is crucial for the mechanism.

3 Model

3.1 Modeling setup

For the realization of the mechanism, a suitable set of geometrical dimensions is required to ensure a well-defined snap-through behavior and to avoid local buckling of the segment. Besides, production constraints have to be considered. Therefore, a parameter study on the geometrical dimensions of the FRE sheet has been carried out in advance until a specific set of geometrical dimensions could be identified, which serves the present purpose. This is not part of the current contribution. The geometrical dimensions used for the simulations are listed in Table 1.

A shell-based approach is aimed for as the thickness of the sheet is two orders of magnitude lower than the other dimensions. Four-node general-purpose shell elements with reduced integration and hourglass control are used for the simulations and three section points over the thickness are considered. The FRE under consideration shows fiber orientations of $\pm 45°$ with respect to the preload direction. The fiber orientations are indicated by the vectors $\mathbf{a}_1$ and $\mathbf{a}_2$ in Figure 1. To mimic the behavior of the weave based reinforcement, an element overlay technique (EOT) is employed. Thereby, two elements share the same nodes and each of them represents an unidirectional reinforced layer. Each layer corresponds to one of the fiber orientations $\mathbf{a}_1$ and $\mathbf{a}_2$, respectively. The interaction between warp and weft yarn on the microscale is not considered at this stage of modeling.

3.2 Material models

To study the influence of the contribution of the fibers of the FRE sheet on the global response, three cases are distinguished for the material models used in the simulations. No fiber contribution gives a lower estimate corresponding to the pure silicone, denoted by PS in the following. The fibers contributing only to the tensile stiffness leads to an intermediate estimate, while fibers contributing also to the compressive stiffness gives an upper estimate, referred to as FRE$^-$ and FRE$^+$, respectively.

For the PS, incompressible material behavior is assumed and an Ogden material law of fourth order is used. Its strain energy density is defined as

$$\psi = \sum_{i=1}^{4} \frac{2\mu_i}{\alpha_i^2} (\lambda_1^{\alpha_i} + \lambda_2^{\alpha_i} + \lambda_3^{\alpha_i} - 3), \tag{1}$$

where λ_j denotes the principal stretch. The material parameters for the fourth order polynomial are α_i and μ_i. These parameters are fitted to experimental data of the matrix material provided by PCCL, Austria, and are summarized in Table 2.

PAMM · Proc. Appl. Math. Mech. **22**:1 (2022)

3 of 6

$i =$	1	2	3	4	C_{10}	k_1	k_2
μ_i	-138.56	69.50	69.51	2.24e-06	0.63575	35.0	52.0
α_i	1.19	1.63	0.75	-11.47			

Table 2 Material parameters for the fourth order Ogden (left) and the HGO model (right).

For the FRE$^-$, the Holzapfel-Gasser-Ogden (HGO) material law available in ABAQUS is used. This material law has been developed for arterial walls in [6,9] and allows to account for the anisotropic hyperelastic material behavior of the FRE$^-$. For incompressible material behavior, no fiber dispersion, and a single family of fibers, the strain energy density reads

$$\psi = C_{10}(\bar{I}_1 - 3) + \frac{k_1}{2k_2} \left(\exp \left[k_2 \langle (\bar{I}_{4(\beta\beta)} - 1) \rangle^2 \right] - 1 \right), \tag{2}$$

where $\bar{I}_1$ denotes the first invariant of the deviatoric part of the right Cauchy-Green stretch tensor, $\bar{\mathbf{C}} = J^{-\frac{2}{3}} \mathbf{C}$. The parameter, $J = \det(\mathbf{F})$, is the determinant of the deformation gradient representing the total volume change. The pseudo-invariant is given as $\bar{I}_{4(\beta\beta)} = \mathbf{a}_\beta \cdot \bar{\mathbf{C}} \mathbf{a}_\beta$, where $\mathbf{a}_\beta$ denotes the vector corresponding to the fiber direction of an unidirectional reinforced layer, where $\beta = 1$ and 2 is used for the EOT approach described in Section 3.1. The Macaulay bracket is defined as $\langle x \rangle = 1/2(|x| + x)$ and deactivates the contribution of the fibers under compression. The material parameters are denoted by C_{10}, k_1, and k_2, which are fitted to experimental data of tensile tests of FRE sheets with fiber orientations of $\pm 45°$ provided by PCCL, Austria. The resulting parameters are summarized in Table 2.

To account for the FRE$^+$, the HGO material law is modified, namely, the Macaulay bracket is omitted. This modification is possible using the user subroutine provided in [4]. Therein, the original HGO material law has been reimplemented and the source code only needs to be changed accordingly. The material parameters used are the same as for the FRE$^-$. This is admissible, as the parameters are based on tensile tests, where the overall stress state is governed by tension.

3.3 Analysis procedure

The analysis procedure slightly differs from the concept of the mechanism introduced in Section 2. The differences arise from computational reasons. Otherwise, convergence difficulties are expected due to the combination of highly nonlinear problems, such as snap-through and contact. The analysis procedure is schematically depicted in Figure 2 and consists of four steps, (i) preload, (ii) snap-through, (iii) equilibration, and (iv) contact step. The Newton-Raphson solution procedure is used for all steps except the snap-through step, for which the modified RIKS arc-length method is employed.

First, the preload step is performed by applying a displacement in 2-direction, U_2^{pre}, on the right edge of the originally flat FRE sheet. Additionally, a small imperfection is applied to let the sheet deform into the desired curved shell structure. The resulting curved shell structure corresponds to the first stable configuration of the snap-through mechanism. This configuration is not stress-free. The displacement, U_2^{pre}, is kept active during all subsequent steps.

The snap-through step is performed by applying torque loads at both edges with opposite signs. The applied torque loads need to be at least large enough to allow the structure to switch to its second stable configuration.

Once the structure is snapped-through, the equilibration step is performed. The applied torque loads at both edges are removed to let the structure find its equilibrium. This equilibrium corresponds to the second stable configuration, which is the counterpart of the first stable configuration mirrored by the 1-2 plane.

The contact step is conducted to determine the clamping force, F_3^{clamp}, of the mechanism. For this purpose, a rigid plate moves towards the structure and comes into contact. The contact between the FRE sheet and the rigid plate is modeled as a surface-to-surface contact without friction involved. For enforcing the contact constraint relationship, the augmented Lagrange method is applied. The reaction force acting on the rigid plate corresponds to the clamping force of the mechanism.

4 Results

In the preload step, a displacement of $U_2^{\text{pre}} = 0.1$ mm is applied on the right edge of each flat sheet, namely, PS, FRE$^-$, and FRE$^+$ sheet. The resulting out-of-plane deformation of the midline of each sheet at $X_1 = L_1/2$ is shown in Figure 3 **a**. This deformation state corresponds to the first stable configuration of the mechanism, exemplified in 3D for the FRE$^+$ sheet in Figure 3 **b**. The first stable configuration slightly deviates from a geometrical perfect cylinder segment as anticlastic bending
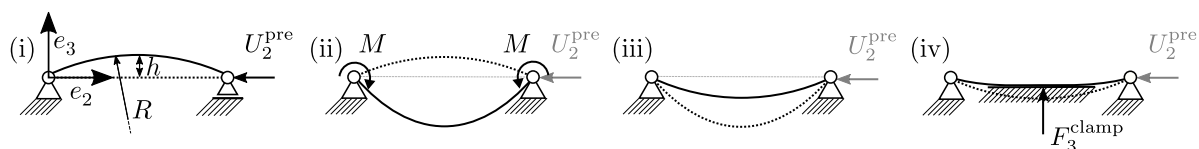

Fig. 2: Schematic of the analysis procedure with (i) preload, (ii) snap-through, (iii) equilibration, and (iv) contact step. The dashed and solid line correspond to the configuration at the beginning and end of each step, respectively.

occurs. The resulting apexes of the midline are quite similar for the different sheets and show values of about 1.2 to 1.4 mm. In contrast, the reaction forces, F_2^{pre}, at the right edge are significantly higher for the FRE$^-$ and FRE$^+$ sheets than for the PS sheet. As expected, the FRE$^+$ sheet shows a higher reaction force than the FRE$^-$ sheet. The numbers can be found in the legend of Figure 3 **a**.

For the snap-through step, the applied torque load over the rotation angle at the right edge is shown for the different sheets in the first row of Figure 4. The equilibrium paths for all sheets are quite complex, especially for the PS. This is indicated by the large number of internal loops of the equilibrium path. The triangle pointing to the right corresponds to the onset of snap-through. At this point, in a torque-controlled design, the structure would dynamically follow a horizontal line to the opposite side of the equilibrium path. In a rotation-controlled design, the structure could follow the unstable equilibrium path until the first hexagon is reached. At this point, the structure would follow a vertical line to the opposite side of the equilibrium path. The unstable equilibrium path between the first and second hexagon corresponds to a snap-back behavior of the structure. Moreover, the equilibrium path of the structure for each material is point symmetric about the origin of the diagram. Hence, the same equilibrium path is obtained for starting from the second stable configuration and reversing the torque loads. For torque load reversal, the onset of snap-through is indicated by the triangle pointing to the left. The torque loads required to let the structure snap-through is significantly higher for the FRE$^-$ and FRE$^+$ sheets than for the PS sheet, where the FRE$^+$ shows the highest value.

The equilibration step is performed, once the structure reaches the onset of snap-through for the torque load reversal, i.e., the triangle pointing to the left. The load torques on both edges are released and the structure find its second stable
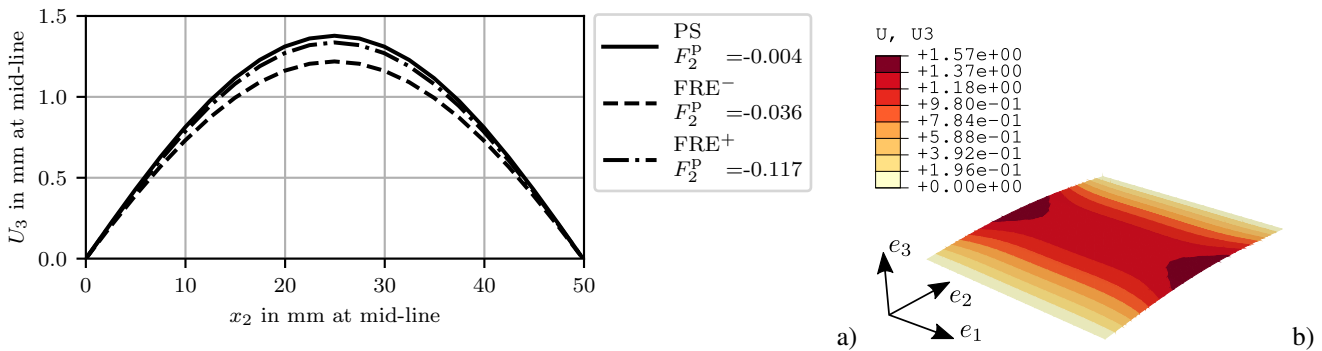

Fig. 3: Out-of-plane displacement, U_3, at the midline of the sheet at $X_1 = L_1/2$ at the end of the preload step **a** and corresponding contour plot of the FRE$^+$ sheet **b**.
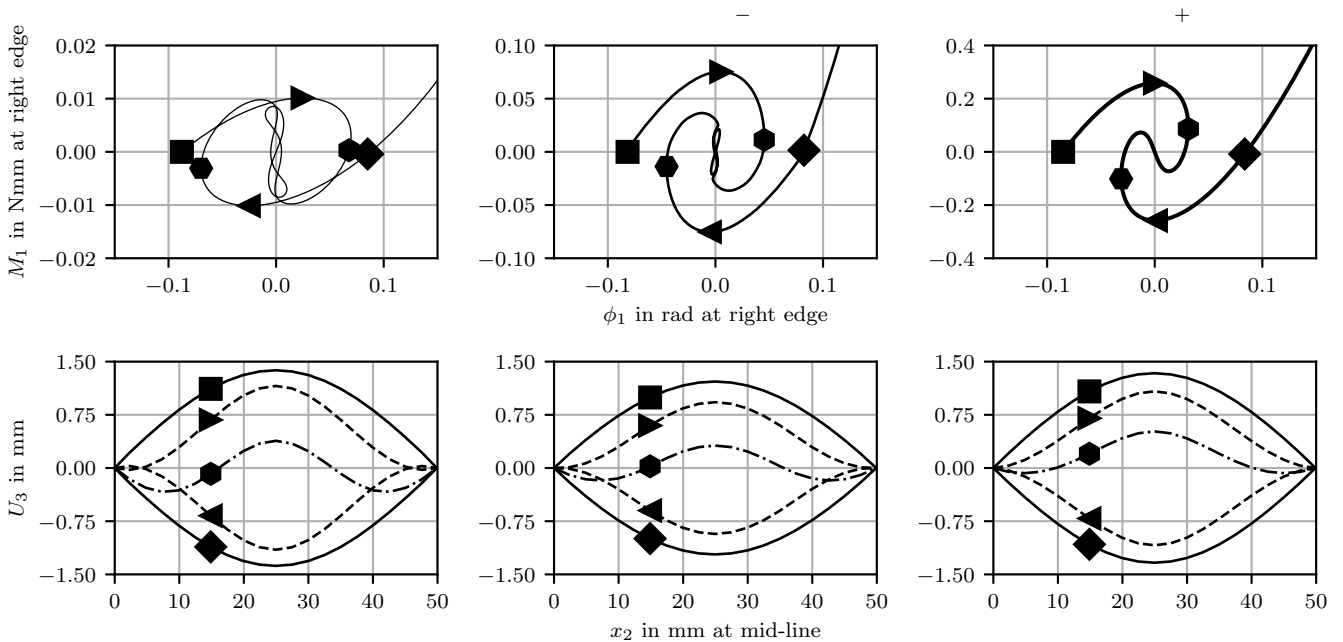

Fig. 4: Torque-rotation curves for the different materials evaluated at the right edge (top) and corresponding deformation of the midline at $X_1 = L_1/2$ (bottom). The first, second, and third column correspond to the PS, FRE$^-$, and FRE$^+$ sheet, respectively. The diagrams for the torque-rotation do not show the same scaling.
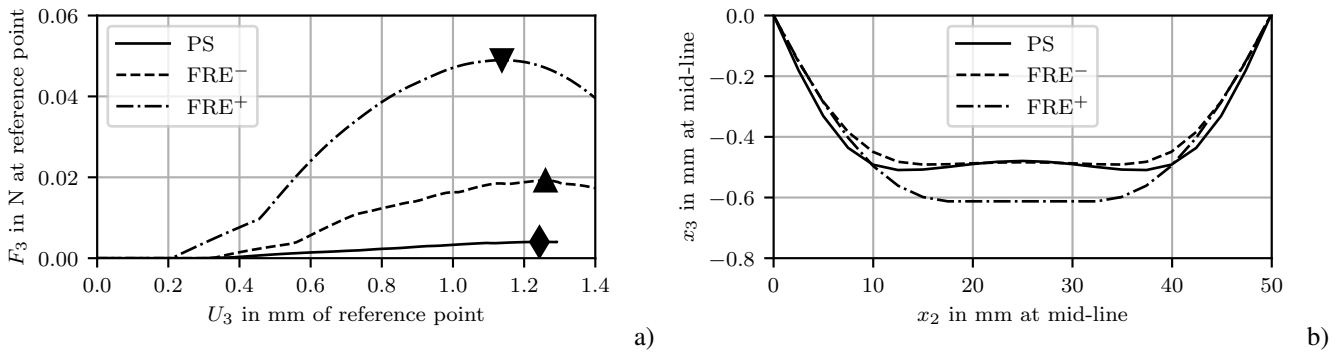
a)

Fig. 5: Contact force, F_3, over displacement, U_3, of rigid plate moving towards structure with markers indicating the maximum clamping forces with ♦ $F_3^{\text{clamp}} = 0.004$, ▲ $F_3^{\text{clamp}} = 0.02$, and ▼ $F_3^{\text{clamp}} = 0.05$ N **a** and corresponding deformation of the midline **b**. The initial position of the rigid plate is located at $X_3 = 2$ mm.
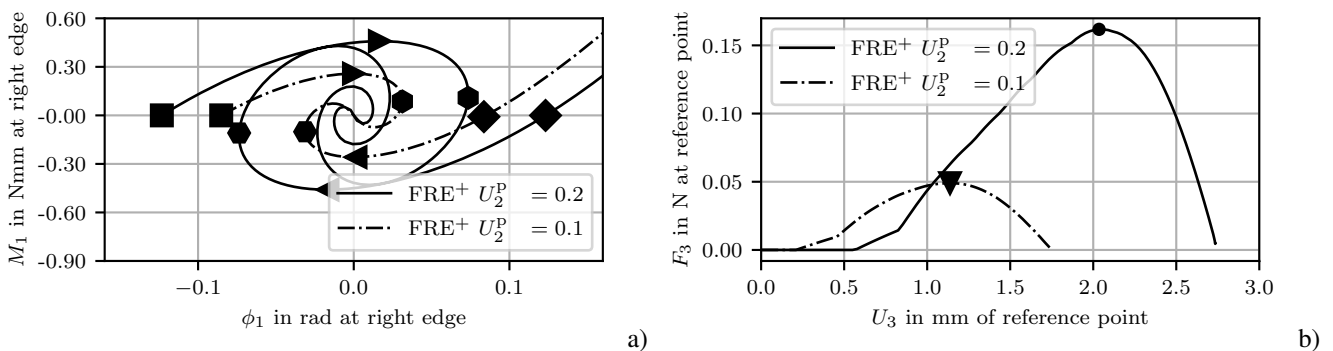

a)

Fig. 6: Torque-rotation curves at right edge for two different preloads of the FRE$^+$ sheet **a**. Contact force, F_3, over displacement, U_3, of rigid plate moving towards structure with markers indicating the maximum clamping force with ▼ $F_3^{\text{clamp}} = 0.05$, ● $F_3^{\text{clamp}} = 0.16$ **b**. The initial position of the rigid plate is located at $X_3 = 2$ mm and $X_3 = 3$ mm for the original and current preload, respectively.

configuration, which is indicated by the diamond in Figure 4. The deformation of the midline at $X_1 = L_1/2$ corresponding to the discussed points on the equilibrium paths is shown in the second row of Figure 4. The patterns are very similar and show the same magnitudes for all sheets.

In order to evaluate the clamping force, the contact step is conducted. The force-displacement diagram corresponding to the reference point of the approaching rigid plate is shown in Figure 5 **a**. The contact force, F_3, at the reference point corresponds to the reaction force acting on the plate and is directly related to the clamping force. It is significantly higher for the FRE$^+$ sheet compared to the other sheets. The markers in the diagram denote the maximum achievable clamping force, F_3^{clamp}, for the different sheets, where the numbers can be found in the Figure caption. The corresponding deformation of the midline for the maximum forces are shown in Figure 5 **b**, where the FRE$^+$ sheet shows the stiffest response compared to the other sheets.

For the initial setup, i.e., $U_2^{\text{pre}} = 0.1$ mm, the resulting values of the clamping forces are rather low for a real application. A straight forward approach is to increase the preload to achieve a higher clamping force. Therefore, the displacement is changed from $U_2^{\text{pre}} = 0.1$ mm to 0.2 mm. For this preload, investigations are performed only for the FRE$^+$ sheet. The results are compared to those obtained for the previous preload.

The apex of the first stable configuration is changing from about 1.34 mm to 1.95 mm, which is not shown for the sake of brevity. The corresponding reaction force in 2-direction at the right edge, F_2^{pre}, is hardly affected, which is expected for this kind of buckling. The torque load to let the structure snap-through for the higher preload is almost twice, cf. Figure 6 **a**. Furthermore, the structure shows a more complex equilibrium path. The force-displacement diagram of the contact step is shown in Figure 6 **b**. The maximum clamping force is about three times higher for the current preload than for the previous one. Based on the successful application of a higher preload, it is shown that the potential for increasing the clamping force can be realized in a simple way. However, increasing the preload is limited as local buckling may become the prevailing instability for higher apexes. Further research is underway to come up with a proper clamping force.

5 Summary

The concept of a simple clamping mechanism based on the snap-through instability of a shallow cylindrical shell segment made from a hyperelastic woven composite is presented. Numerical simulations by means of the FEM are performed to show

the feasibility of the concept. A material model for the pure matrix and two different material models for the composite, which take into account whether or not the fibers contribute to the compressive stiffness, are used to estimate the contribution of the fibers to the structural response of the mechanism. The maximum resulting clamping forces are evaluated for all three materials.

The simulations show that the presented concept using the snap-through behavior of an anisotropic hyperelastic shallow cylindrical shell segment is feasible. The contribution of the fibers has a significant influence on the overall structural response and leads to higher clamping forces than for the pure matrix. The highest clamping force can be achieved for the case of fibers contributing under compression, while it is an order of magnitude lower for the pure matrix material. This highlights the importance of the contribution of the reinforcement to achieve an adequate stiffness of the mechanism. For the initial setup, the extracted clamping forces are markedly below those of a desired application. To increase the clamping force of the mechanism, it is necessary to change either the composition of the constituents, geometrical dimensions of the FRE sheet, or changing the preload. First results considering higher preloads are promising. The clamping force is three times higher than for the original preload. This shows the potential of the present concept to increase the clamping force by various parameters in a simple way.

References

[1] J. Beter, B. Schrittesser, B. Maroh, E. Sarlin, P. F. Fuchs, and G. Pinter, Polymers **12(2)**, 1–11 (2020).
[2] J. Beter, B. Schrittesser, G. Meier, P. F. Fuchs, and G. Pinter, Appl. Compos. Mater. **27(3)**, 149–164 (2020).
[3] J. Beter, B. Maroh, B. Schrittesser, I. Mühlbacher, T. Griesser, S. Schlögl, P. F. Fuchs, and G. Pinter, Polymers **13(1)**, 1–17 (2021).
[4] H. Fehervary, L. Maes, J. Vastmans, G. Kloosterman, and N. Famaey, J. Mech. Behav. Biomed. Mater. **110**, 103737 (2020).
[5] A. Galley, G. K. Knopf, M. Kashkoush, Actuators **8**, 76 (2019).
[6] T. C. Gasser, R. W. Ogden, and G. A. Holzapfel, J. R. Soc. Interface **3(6)**, 15–35 (2006).
[7] P. Giddings C. R. Bowen, R. Butler, H. A. Kim Compos. - A: Appl. Sci. Manuf. **39**, 697–703 (2008).
[8] R. M. J. Groh, and A. Pirrera Compos. Struct. **198**, 63–72 (2018).
[9] G. A. Holzapfel, T. C. Gasser, and R. W. Ogden J. Elast. **61**, 1–48 (2000).
[10] M. R. Schultz, M. W. Hyer, R. Brett Williams, W. Keats Wilkie, and D. J. Inmand Compos. Struct. **66**, 2442–2448 (2006).
[11] J. Shintake, V. Cacucciolo, D. Floreano, and H. Shea Adv. Mater. **30**, 1707035 (2018).
[12] Y. Zhou, I. Stanciulescu, T. Eason, and M.Spottswood Finite Elem Anal Des **96**, 41–50 (2015).